

# Polarization of neutron star surface emission: a systematic analysis

R. Taverna<sup>1\*</sup>, R. Turolla<sup>1,2</sup>, D. Gonzalez Caniulef<sup>2</sup>, S. Zane<sup>2</sup>, F. Muleri<sup>3</sup>, P. Soffitta<sup>3</sup>

<sup>1</sup>*Department of Physics and Astronomy, University of Padova, via Marzolo 8, 35131 Padova, Italy*

<sup>2</sup>*Mullard Space Science Laboratory, University College London, Holmbury St. Mary, Surrey, RH5 6NT, UK*

<sup>3</sup>*INAF-IASF Roma, Via del Fosso del Cavaliere 100, 00133 Roma, Italy*

Accepted . . . . Received . . . ; in original form . . .

## ABSTRACT

New-generation X-ray polarimeters currently under development promise to open a new window in the study of high-energy astrophysical sources. Among them, neutron stars appear particularly suited for polarization measurements. Radiation from the (cooling) surface of a neutron star is expected to exhibit a large intrinsic polarization degree due to the star strong magnetic field ( $\approx 10^{12}$ – $10^{15}$  G), which influences the plasma opacity in the outermost stellar layers. The polarization fraction and polarization angle as measured by an instrument, however, do not necessarily coincide with the intrinsic ones derived from models of surface emission. This is due to the effects of quantum electrodynamics in the highly magnetized vacuum around the star (the vacuum polarization) coupled with the rotation of the Stokes parameters in the plane perpendicular to the line of sight induced by the non-uniform magnetic field. Here we revisit the problem and present an efficient method for computing the observed polarization fraction and polarization angle in the case of radiation coming from the entire surface of a neutron star, accounting for both vacuum polarization and geometrical effects due to the extended emitting region. Our approach is fairly general and is illustrated in the case of blackbody emission from a neutron star with either a dipolar or a (globally) twisted magnetic field.

**Key words:** magnetic fields — polarization — stars: neutron — techniques: polarimetric

## 1 INTRODUCTION

Polarization measurements of radiation coming from astrophysical sources helped in improving our knowledge about the physical and geometrical properties of a variety of systems, from black holes to gamma-ray bursts (e.g. Trippe 2014, for a review). In this respect, neutron stars (NSs) are among the most promising targets for polarimetry due to their strong magnetic field which is expected to induce a large degree of polarization of the emitted radiation.

Radio and optical polarimetry has been already used to derive the orientation of the magnetic and rotation axes of radio pulsars (Manchester & Taylor 1977; Lyne & Manchester 1988; see also Pavlov & Zavlin 2000). The discovery over the last two decades of new classes of X-ray bright, radio-silent NSs with very faint (if any) optical counterparts (chiefly the magnetar candidates, e.g. Mereghetti 2008; Turolla, Zane & Watts 2015, and the X-ray Dim Isolated Neutron Stars, XDINSs, e.g. Turolla 2009; Kaspi 2010) renewed the interest in possible polarization measurements at X-ray energies in NS sources. Despite some efforts were made in the past to measure polarization in the X-rays, mainly with the OSO-8 and INTEGRAL satellites (Weisskopf et al. 1978; Hughes et al. 1984;

Dean et al. 2008; see also Kislat et al. 2015), the poor sensitivity of past instrumentation did not lead to conclusive results. A new window opened in the last years, with the advent of new-generation X-ray polarimeters, like XIPE<sup>1</sup>, IXPE and PRAXyS<sup>2</sup> (recently selected for the study phase of the ESA M4 and NASA SMEX programmes respectively), which are based on the photoelectric effect and provide a dramatic increase in sensitivity over an energy range  $\sim 1$ –30 keV (see Bellazzini et al. 2013). X-ray polarimeters derive polarization observables by detecting a modulation in the azimuthal distribution of events in the focal plane. Actually, while a measure of the circular polarization degree is possible in the optical band (see e.g. Wiktorowicz et al. 2015), current instruments, based on the photoelectric effect or Compton scattering, can only provide information about linear polarization (Fabiani & Muleri 2014).

From a theoretical viewpoint, polarization observables (the polarization fraction and the polarization angle) are conveniently expressed through the Stokes parameters. The comparison between the polarization properties of the photons emitted at the source and those measured at earth is not straightforward for two main reasons.

<sup>1</sup> <http://www.isdc.unige.ch/xipe>

<sup>2</sup> Weisskopf et al. (2013), Jahoda et al. (2015)

\* E-mail: taverna@pd.infn.it

The first is that the Stokes parameters are defined with respect to a given frame, which is in general different for each photon. When the Stokes parameters relative to the different photons are added together, care must be taken to rotate them, so that they are referred to the same frame, which coincides with the frame in the focal plane of the detector. This effect becomes important every time radiation comes from a spatial region endowed with a non-constant magnetic field, and will be referred to as “geometrical effect” in the following. The second issue, which typically arises in NSs, is related to “vacuum polarization”. In the presence of a strong magnetic field, quantum electrodynamics (QED) alters the dielectric and magnetic properties of the vacuum outside the star, substantially affecting polarization (Heyl & Shaviv 2002). Because of this, (100% linearly polarized) photons emitted by the surface will keep their polarization state up to some distance from the star, as they propagate adiabatically. This implies that the degree of polarization and the polarization angle, as measured at infinity, depend also on the extension of the “adiabatic region”, which in turn depends on the photon energy and on the magnetic field.

The observed polarization properties of radiation from isolated NSs were investigated in the past both in connection with the emission from the cooling star surface and the reprocessing of photons by magnetospheric electrons through resonant Compton scattering, a mechanism which is thought to operate in magnetars. Pavlov & Zavlin (2000) studied the case of thermal emission from the entire surface of a NS covered by an atmosphere, without accounting for QED and geometrical effects. A quite complete analysis of the observed polarization properties of surface emission from a neutron star has been presented by Heyl, Shaviv & Lloyd (2003), while Lai & Ho (2003) and van Adelsberg & Perna (2009) focused on the role played by the vacuum resonance<sup>3</sup>, which occurs in the dense atmospheric layers, on the polarization, and may provide a direct observational signature of vacuum polarization. The two latter works were restricted to the case of emission from a small hot spot on the NS surface, over which the magnetic field can be treated as uniform, therefore no account for rotation of the Stokes parameters was required. Fernández & Davis (2011) and Taverna et al. (2014) have shown that X-ray polarization measurements can provide independent estimates of the geometrical and physical parameters and probe QED effects in the strong field limit in magnetar sources.

In this paper we re-examine the problem and present a simplified, efficient method to derive the observed polarization properties of radiation emitted from the entire surface of a NS. Our results are in agreement with those of Heyl, Shaviv & Lloyd (2003) and van Adelsberg & Perna (2009), and our faster approach allows to systematically explore the dependence of the polarization observables on the different geometrical and physical quantities. In particular, we discuss the difference between the polarization properties of the radiation emitted by the star and those measured at earth, which is induced by geometrical and QED effects. This aspect, which is crucial when one needs to reconstruct the star properties from the observed quantities, has not been systematically investigated in previous works. A complete study based on physically consistent models of surface emission is outside the scope of this analysis, and we just assume a simple model in which the surface emission is a (isotropic) blackbody and the magnetic field is dipolar

(or a globally twisted dipole field). The outline of the paper is as follows. The theoretical framework is introduced in section 2. In section 3 calculations and results are presented, while section 4 contains a discussion about our findings and the conclusions.

## 2 THEORETICAL OVERVIEW

In this section we briefly summarize some basic results about the evolution of the polarization state of electromagnetic radiation propagating in a strongly magnetized vacuum. Although the considerations we present below are focused on radiation travelling in the surroundings of a neutron star, they hold quite in general.

### 2.1 Photon polarization in strong magnetic fields

In the presence of strong magnetic fields photons are linearly polarized in two normal modes: the ordinary mode (O-mode), in which the electric field oscillates in the plane of the propagation vector  $\mathbf{k}$  and the local magnetic field  $\mathbf{B}$ , and the extraordinary mode (X-mode), in which, instead, the electric field oscillates perpendicularly to both  $\mathbf{k}$  and  $\mathbf{B}$ . This holds for photon energies below the electron cyclotron energy ( $E < E_{ce} = \hbar e B / m_e c \simeq 11.6 (B/10^{12} \text{ G}) \text{ keV}$ ; Gnedin & Pavlov 1974), which implies  $B \gtrsim 10^{11} \text{ G}$  at X-ray energies, whereas  $B$  can be as low as  $\sim 10^{10} \text{ G}$  in the optical band. Moreover, the polarization state of photons propagating in vacuo is also influenced by the effects of vacuum polarization (Heyl & Shaviv 2000, 2002, Harding & Lai 2006). According to QED, in fact, photons can temporarily convert into virtual  $e^\pm$  pairs. The strong magnetic field polarizes the pairs, modifying the dielectric,  $\epsilon$ , and magnetic permeability,  $\mu$ , tensors of the vacuum, which would coincide with the unit tensor otherwise.

Fixing a reference frame  $(x, y, z)$  with the  $z$ -axis along the photon propagation direction  $\mathbf{k}$ , and the  $x$ -axis perpendicular to both  $\mathbf{k}$  and the local magnetic field  $\mathbf{B}$ , the evolution of the wave electric field is governed by the following system of differential equations (see Fernández & Davis 2011; Taverna et al. 2014; see also Heyl & Shaviv 2002 for a different, albeit equivalent, formulation)

$$\begin{aligned} \frac{dA_x}{dz} &= \frac{ik_0\delta}{2}(MA_x + PA_y) \\ \frac{dA_y}{dz} &= \frac{ik_0\delta}{2}(PA_x + NA_y). \end{aligned} \quad (1)$$

Here  $\mathbf{A} = (A_x, A_y) = (a_x e^{-i\varphi_x}, a_y e^{-i\varphi_y})$  is the electric field complex amplitude,  $k_0 = \omega/c$  with  $\omega$  the photon angular frequency and the adimensional quantities  $\delta$ ,  $M$ ,  $N$  and  $P$  depend on the (local) magnetic field strength; in particular it is  $\delta = (\alpha_F/45\pi)(B/B_Q)^2$ , where  $\alpha_F$  is the fine structure constant and  $B_Q = 4.4 \times 10^{13} \text{ G}$  is the critical magnetic field. As equations (1) show, vacuum polarization induces a change in the electric field as the wave propagates: the typical lengthscale over which this occurs is  $\ell_A = 2/k_0\delta \simeq 100(B/10^{11} \text{ G})^{-2}(E/1 \text{ keV})^{-1} \text{ cm}$ , where  $E = \hbar\omega$ . At the same time, the magnetic field changes along the photon trajectory, this time over a lengthscale  $\ell_B = B/|\mathbf{k} \cdot \nabla B| \sim r$ , where  $r$  is the radial distance. Near to the star surface it is  $\ell_A \ll \ell_B$  and the direction along which the wave electric field oscillates can instantaneously adapt to the variation of the local magnetic field direction, maintaining the original polarization state. In these conditions, the photon is said to

<sup>3</sup> A Mikheyev-Smirnov-Wolfenstein resonance which may induce mode conversion in X-ray photons for typical magnetar-like fields ( $B \gtrsim 10^{14} \text{ G}$ ).

propagate adiabatically and in the following we will refer to the region in which this occurs as the adiabatic region. However, as the photon moves outwards the magnetic field strength decreases ( $B \propto r^{-3} \sqrt{1 + 3 \cos^2 \theta}$  for a dipole field, where  $\theta$  is the magnetic colatitude) and  $\ell_A$  increases. Since  $\ell_B$  grows more slowly, there is an intermediate region in which the wave electric field can not promptly follow the variation of the magnetic field any more. Finally, in the external region, where  $\ell_A \gg \ell_B$ , the electric field direction freezes, and the polarization modes change as the magnetic field direction varies along the photon trajectory.

The evolution of the polarization modes should be calculated integrating equations (1) from the surface up to infinity (or, at least, up to a distance sufficiently large to consider the complex amplitude components  $A_x$  and  $A_y$  as constants). This has been the approach followed by Heyl, Shaviv & Lloyd (2003, see also Fernández & Davis 2011; Taverna et al. 2014). However, this method requires quite long computational times, since numerical integration must be carried on along each ray and it is not particularly suited for a systematic study of how the polarization observables depend on the various physical and geometrical parameters. Since the latter is the main goal of the present work, we resort to a simpler, approximated treatment in which only the adiabatic region and the external one are included, and they are divided by a sharp edge. To this end we introduce the adiabatic radius<sup>4</sup>  $r_a$ , defined implicitly by the condition  $\ell_A = \ell_B$ . Assuming a dipole field and purely radial photon trajectories, it is  $\ell_B = r/3$  and hence  $\ell_A(r_a) = r_a/3$ . Recalling the expression for  $\ell_A$ , it follows that  $r_a/R_{\text{NS}} \simeq 3.9 \times 10^{-4} (E/1 \text{ keV})^{-1} (B_P/10^{11} \text{ G})^{-2} (R_{\text{NS}}/r_a)^{-6}$  and finally

$$r_a \simeq 4.8 \left( \frac{B_P}{10^{11} \text{ G}} \right)^{2/5} \left( \frac{E}{1 \text{ keV}} \right)^{1/5} R_{\text{NS}}, \quad (2)$$

where  $R_{\text{NS}}$  is the stellar radius,  $B_P$  is the polar strength of the dipole and  $\cos \theta \sim 1$  was assumed. The adiabatic radius depends on both the photon energy and the star magnetic field: it is larger for stars with stronger magnetic field, and, at fixed  $B_P$ , it becomes smaller for less energetic photons, as shown in Figure 1.

## 2.2 Polarized radiative transfer

A convenient way to describe the polarization properties of the radiation emitted by a source is through the Stokes parameters. With reference to the frame  $(x, y, z)$  introduced in Section 2.1, they are related to the complex components of the wave electric field by

$$\begin{aligned} \mathcal{I} &= A_x A_x^* + A_y A_y^* = a_x^2 + a_y^2 \\ \mathcal{Q} &= A_x A_x^* - A_y A_y^* = a_x^2 - a_y^2 \\ \mathcal{U} &= A_x A_y^* + A_y A_x^* = 2a_x a_y \cos(\varphi_x - \varphi_y) \\ \mathcal{V} &= i (A_x A_y^* - A_y A_x^*) = 2a_x a_y \sin(\varphi_x - \varphi_y). \end{aligned} \quad (3)$$

In the previous equations a star denotes the complex conjugate,  $\mathcal{I}$  is the total intensity of the wave associated to the photon,  $\mathcal{Q}$  and  $\mathcal{U}$  describe the linear polarization and  $\mathcal{V}$  the circular polarization. The four Stokes parameters satisfy the general relation  $\mathcal{I}^2 \geq \mathcal{Q}^2 + \mathcal{U}^2 + \mathcal{V}^2$ , the equality holding for 100% polarized radiation. With our

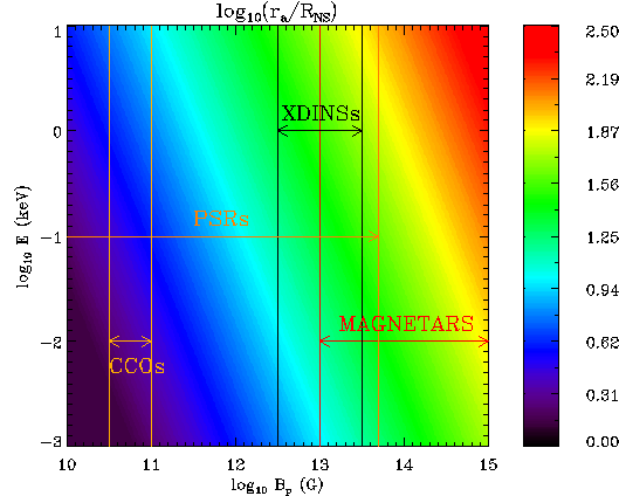


**Figure 1.** Contour plot showing the adiabatic radius  $r_a$  (in units of the stellar radius  $R_{\text{NS}}$ ) as a function of the polar magnetic field strength and the photon energy. The typical  $B_P$ -ranges for different classes of neutron stars, the magnetars, the isolated, thermally emitting NSs (XDINSs), the radio-pulsars (PSRs) and the central compact objects (CCOs), are also shown.

current choice of the reference frame, it is  $a_y = 0$  for an X-mode photon and  $a_x = 0$  for an O-mode photon. Normalizing the Stokes parameters defined above to the intensity  $\mathcal{I}$ , we can associate to an extraordinary/ordinary photon the vectors

$$\begin{pmatrix} \bar{\mathcal{Q}} \\ \bar{\mathcal{U}} \\ \bar{\mathcal{V}} \end{pmatrix}_X = \begin{pmatrix} 1 \\ 0 \\ 0 \end{pmatrix} \quad \begin{pmatrix} \bar{\mathcal{Q}} \\ \bar{\mathcal{U}} \\ \bar{\mathcal{V}} \end{pmatrix}_O = \begin{pmatrix} -1 \\ 0 \\ 0 \end{pmatrix}, \quad (4)$$

where a bar denotes the normalized Stokes parameters. The evolution of the Stokes parameters mirrors that of the complex components of the electric field given in equations (1) (see e.g. Taverna et al. 2014). Actually, in our hypothesis of 100% linearly polarized thermal radiation, the Stokes parameter  $\mathcal{V}$  is always zero inside the adiabatic region. This implies that a circular polarization degree can arise only as a consequence of the polarization mode evolution in the transition between the adiabatic and the external region. However, since we do not integrate equations (1) in our model we will not discuss  $\mathcal{V}$  further. We verified that, even accounting for the Stokes parameter evolution, as obtained solving equations (1) across the entire region, the resulting circular polarization fraction is very small at optical energies and reaches at most a few percent in the X-ray band.

In order to measure the polarization properties of a given source, a polarimeter will collect a large number of photons, each characterized by its own set of Stokes parameters. The convenience of using the Stokes parameters lies precisely in the fact that they are additive (e.g. Rybicki & Lightman 2004): the Stokes parameters associated to the whole collected radiation (i.e. the superposition of all the received photons) are equal to the sum of the Stokes parameters of the single photons. However, care must be taken since the quantities in equations (3) are defined with respect to a precise reference frame,  $(x, y, z)$ , that depends on the direction of the local magnetic field  $\mathbf{B}$  (see §2.1). As the magnetic field is in general non-uniform across the emission region, its direction at a given point will depend on the source magnetic topology. Since the direction of the electric field of each photon varies very quickly inside the adiabatic region, but it is frozen outside, what actually matters is not the

<sup>4</sup> This same quantity is called the polarization-limiting radius,  $r_{\text{pl}}$ , in previous literature (see Heyl & Shaviv 2002).

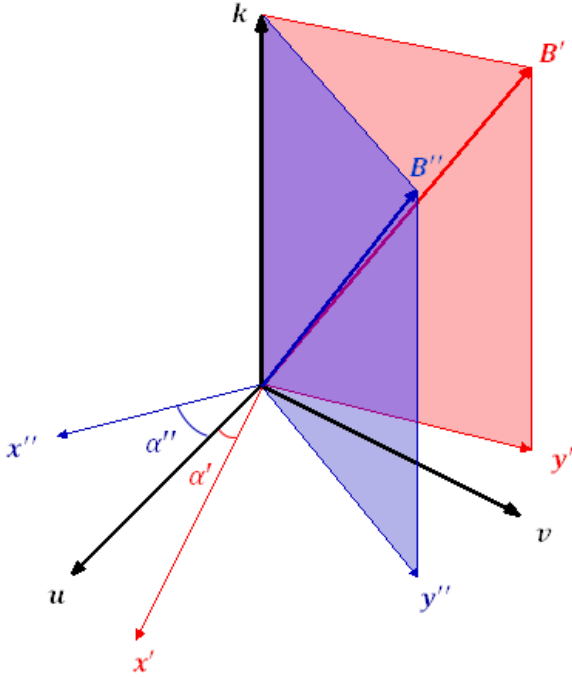


**Figure 2.** Graphical visualization of the different reference frames introduced in the text.  $\mathbf{k}$  is the common direction of propagation (LOS);  $(\mathbf{u}, \mathbf{v})$  are the fixed, mutually orthogonal axes of the polarimeter;  $(\mathbf{x}', \mathbf{y}')$  and  $(\mathbf{x}'', \mathbf{y}'')$  are mutually orthogonal axes of two reference frames relative to photons coming from points characterized by the directions  $\mathbf{B}'$  and  $\mathbf{B}''$  of the magnetic field. The angles  $\alpha'$ ,  $\alpha''$  are also indicated.

$B$ -field direction at the original emission point, but that at the point where the photon crosses the adiabatic boundary  $r_a$ , as pointed out by Lai & Ho (2003). Let us call  $(x_i, y_i, z_i)$  the reference frame in which the Stokes parameters associated to the generic photon are defined at the adiabatic radius. While the  $z_i$  axes are all along the same direction (that coincides with the observer line-of-sight, LOS), the  $x_i$  and  $y_i$  axes will point, in general, in different directions for each photon (see Figure 2). To sum correctly the Stokes parameters it is necessary to refer them to the same, fixed frame, say  $(u, v, w)$ . This frame can be chosen in such a way to coincide with that of the polarimeter, with  $u$  and  $v$  in the detector plane and  $w$  along the LOS.

Each reference frame  $(x_i, y_i, z_i)$  is rotated with respect to the fixed,  $(u, v, w)$ , frame by an angle  $\alpha_i$  around the common  $z_i \equiv w$  axis, where  $\cos \alpha_i = \mathbf{u} \cdot \mathbf{x}_i$ . Under a rotation of the reference frame by an angle  $\alpha_i$ , the Stokes parameters transform as

$$\begin{aligned} I_i &= \bar{I}_i \\ Q_i &= \bar{Q}_i \cos(2\alpha_i) + \bar{U}_i \sin(2\alpha_i) \\ U_i &= \bar{U}_i \cos(2\alpha_i) - \bar{Q}_i \sin(2\alpha_i). \end{aligned} \quad (5)$$

Since photons emitted by the star surface, or, more generally, inside the adiabatic region, are 100% polarized either in the X or O mode (i.e.  $\bar{Q}_i = \pm 1$  and  $\bar{U}_i = 0$ ), the Stokes parameters of the radiation collected at infinity are

$$\begin{aligned} Q &= \sum_{i=1}^N Q_i = \sum_{i=1}^{N_X} \cos(2\alpha_i) - \sum_{j=1}^{N_O} \cos(2\alpha_j) \\ U &= \sum_{i=1}^N U_i = \sum_{j=1}^{N_O} \sin(2\alpha_j) - \sum_{i=1}^{N_X} \sin(2\alpha_i) \end{aligned} \quad (6)$$

where  $N_X$  ( $N_O$ ) is the number of extraordinary (ordinary) photons,  $N = N_X + N_O$ , and we used equations (5).

### 2.3 Polarization observables

The polarization state of the detected radiation can be described in terms of two observables<sup>5</sup>, the linear polarization fraction  $\Pi_L$  and the polarization angle  $\chi_p$  defined as

$$\begin{aligned} \Pi_L &= \frac{\sqrt{Q^2 + U^2}}{I} \\ \chi_p &= \frac{1}{2} \arctan \left( \frac{U}{Q} \right). \end{aligned} \quad (7)$$

The linear polarization fraction is not, in general, equivalent to the ratio  $|N_X - N_O|/N$  (as previously noticed by Heyl, Shaviv & Lloyd 2003). This would happen only if all the angles  $\alpha_i$  were the same, i.e. when the magnetic field is uniform across the emitting region (as in the case considered by Lai & Ho 2003 and van Adelsberg & Perna 2009 of radiation coming from a small hot spot on the NS surface). In fact, denoting with  $\alpha_0$  the common value and substituting expressions (6) in the first of equations (7), one obtains

$$\begin{aligned} \Pi_L &= \frac{\sqrt{(N_X - N_O)^2 \cos^2(2\alpha_0) + (N_O - N_X)^2 \sin^2(2\alpha_0)}}{N} \\ &= \frac{|N_X - N_O|}{N}. \end{aligned} \quad (8)$$

Under the same hypothesis the polarization angle, given by the second of equations (7), is directly related to the angle  $\alpha_0$

$$\chi_p = \frac{1}{2} \arctan \left[ \frac{(N_O - N_X) \sin(2\alpha_0)}{(N_X - N_O) \cos(2\alpha_0)} \right] = -\alpha_0. \quad (9)$$

Hence, the polarization fraction gives direct information about the intrinsic degree of polarization of the radiation (i.e. that at the source) only for a constant rotation angle  $\alpha_0$ . Under the same conditions, the polarization angle provides the direction of the (uniform) magnetic field of the source in the plane of the sky.

On the contrary, if the  $B$ -field is non-uniform (e.g. for emission coming from the entire surface of a NS endowed with a dipole field),  $\alpha$  will vary according to the magnetic field direction at the point where the photon crosses the adiabatic radius. In this case equations (6) and (7) give

$$\begin{aligned} \Pi_L &= \frac{1}{N} \left[ N + 2 \sum_i \sum_{k>i} \cos(2\alpha_i - 2\alpha_k) \right. \\ &\quad + 2 \sum_j \sum_{r>j} \cos(2\alpha_j - 2\alpha_r) \\ &\quad \left. - 2 \sum_i \sum_j \cos(2\alpha_i - 2\alpha_j) \right]^{1/2}, \end{aligned} \quad (10)$$

where  $i, k = 1, \dots, N_X$  and  $j, r = 1, \dots, N_O$ , while the polarization angle results in

$$\chi_p = \frac{1}{2} \arctan \left[ - \frac{\sum_{i=1}^{N_X} \sin(2\alpha_i) - \sum_{j=1}^{N_O} \sin(2\alpha_j)}{\sum_{i=1}^{N_X} \cos(2\alpha_i) - \sum_{j=1}^{N_O} \cos(2\alpha_j)} \right]. \quad (11)$$

So, in the general case both  $\Pi_L$  and  $\chi_p$  depend on the distribution of the angles  $\alpha_i$ , which, in turn, is determined by the geometry of the magnetic field.

<sup>5</sup> As mentioned earlier, circular polarization is not considered in the present work.

### 3 POLARIZATION OF SURFACE EMISSION FROM NEUTRON STARS

In this section we present quantitative results for the polarization observables in the case of surface (thermal) emission from a neutron star endowed with an axially-symmetric magnetic field, either a dipole or a (globally) twisted dipole, the latter often used to describe the magnetosphere of magnetars (see Thompson, Lyutikov & Kulkarni 2002).

#### 3.1 The $\alpha$ -distribution

Let us introduce a reference frame  $(X, Y, Z)$  with the  $Z$ -axis in the direction of the LOS (unit vector  $\ell$ ),  $\mathbf{X}$  in the plane of  $\ell$  and the star spin axis (unit vector  $\Omega$ ) and  $\mathbf{Y} = \ell \times \mathbf{X}$ . The geometry is shown in Figure 3a, where  $\chi$  is the angle between the spin axis and the LOS, and  $\xi$  is the angle between the spin axis and the magnetic dipole axis (unit vector  $\mathbf{b}_{\text{dip}}$ ). It is  $\Omega = (-\sin \chi, 0, \cos \chi)$  while, having introduced the polar angles  $\eta$  and  $\zeta$  that fix the direction of  $\mathbf{b}_{\text{dip}}$  with respect to  $\ell$  (see again Figure 3a), one has  $\mathbf{b}_{\text{dip}} = (\sin \eta \cos \zeta, \sin \eta \sin \zeta, \cos \eta)$ . The angles  $\eta$  and  $\zeta$  are related to  $\chi$  and  $\xi$  by

$$\begin{aligned} \cos \eta &= \cos \chi \cos \xi + \sin \chi \sin \xi \cos \gamma \\ \cos \zeta &= \frac{\cos \xi - \cos \chi \cos \eta}{\sin \chi \sin \eta}, \end{aligned} \quad (12)$$

where  $\gamma$  is the rotational phase. Using the previous expressions, the components of the unit vector  $\mathbf{b}_{\text{dip}}$  in the frame  $(X, Y, Z)$  become

$$\mathbf{b}_{\text{dip}} = \begin{pmatrix} \sin \chi \cos \xi - \cos \chi \sin \xi \cos \gamma \\ \sin \xi \sin \gamma \\ \cos \chi \cos \xi + \sin \chi \sin \xi \cos \gamma \end{pmatrix}. \quad (13)$$

According to the discussion in §2.2, the axes  $u$  and  $v$  of the polarimeter frame can be chosen as any pair of orthogonal directions in the  $XY$  plane. In general it is

$$\mathbf{u} \equiv \mathbf{X} = \begin{pmatrix} \cos \psi \\ \sin \psi \\ 0 \end{pmatrix}, \quad \mathbf{v} \equiv \mathbf{Y} = \begin{pmatrix} -\sin \psi \\ \cos \psi \\ 0 \end{pmatrix}. \quad (14)$$

where  $\psi$  is the angle that the  $u$  axis makes with the  $X$  axis. The axes  $x$  and  $y$  of the reference frame  $(x, y, z)$ , that change for each photon, are defined once the magnetic field geometry is fixed as

$$\mathbf{x} = \frac{\ell \times \mathbf{B}}{|\ell \times \mathbf{B}|}, \quad \mathbf{y} = \ell \times \mathbf{x}. \quad (15)$$

The angle  $\alpha$  by which the photon frame  $(x, y, z)$  has to be rotated to coincide with the polarimeter frame  $(u, v, w)$  is then simply obtained taking the scalar product of  $\mathbf{u}$  with  $\mathbf{x}$

$$\cos \alpha = \mathbf{u} \cdot \mathbf{x}. \quad (16)$$

The indetermination in the sign of  $\alpha$  is resolved looking at the sign of  $\mathbf{v} \cdot \mathbf{x}$ ; if the latter is positive the rotation is by an angle  $-\alpha$  (i.e.  $\sin \alpha = -\sqrt{1 - \cos^2 \alpha}$ ).

Since we need to consider photons only from the boundary of the adiabatic region outwards,  $\mathbf{B}$  in the first of equations (15) is the stellar magnetic field calculated at  $r_a$  (see equation 2). Actually, it is more convenient to express the magnetic field components in a reference frame  $(p, q, t)$ , with the  $t$  axis along  $\mathbf{b}_{\text{dip}}$  and  $p, q$  two mutually orthogonal directions in the plane perpendicular to  $t$  (see Figure 3b). For a dipole, in particular, the polar components of the

magnetic field in this frame are

$$\mathbf{B}^{\text{pol}} = \begin{pmatrix} B_r \\ B_\theta \\ B_\phi \end{pmatrix} = \frac{B_P}{2} \left( \frac{R_{\text{NS}}}{r_a} \right)^3 \begin{pmatrix} 2 \cos \theta \\ \sin \theta \\ 0 \end{pmatrix}, \quad (17)$$

where  $\theta$  is the magnetic colatitude. Then, the cartesian components  $\mathbf{B} = (B_p, B_q, B_t)$  can be calculated making use of expressions (A3) in Appendix A. However, since all the calculations to derive the analytical expression of the angle  $\alpha$  (see equation 16) are in the LOS reference frame, the  $X, Y$  and  $Z$  components of  $\mathbf{B}$  are needed. They can be obtained through a change of basis as

$$\begin{aligned} B_X &= B_p p_X + B_q q_X + B_t (b_{\text{dip}})_X \\ B_Y &= B_p p_Y + B_q q_Y + B_t (b_{\text{dip}})_Y \\ B_Z &= B_p p_Z + B_q q_Z + B_t (b_{\text{dip}})_Z, \end{aligned} \quad (18)$$

where the components of  $\mathbf{p}$ , and  $\mathbf{q}$  in the  $(X, Y, Z)$  frame are given in Appendix B, while those of  $\mathbf{b}_{\text{dip}}$  are given by equation (13).

Substituting the expressions (18) in the first of equations (15), the components of the unit vector  $\mathbf{x}$  in the LOS reference frame are

$$\mathbf{x} = \frac{1}{\sqrt{B_X^2 + B_Y^2}} \begin{pmatrix} -B_Y \\ B_X \\ 0 \end{pmatrix}. \quad (19)$$

$B_X$  and  $B_Y$  clearly depend on the angles  $\chi, \xi$  and the phase  $\gamma$  through the unit vectors of the  $(p, q, t)$  reference frame, given by equations (B2), (B3) and (13). Moreover, they depend also on the magnetic colatitude and azimuth ( $\theta$  and  $\phi$  that fix the point where the magnetic field is calculated on the adiabatic surface) through the components  $B_p, B_q$  and  $B_t$  given by equations (A3) and (17). Actually, the angles  $\theta$  and  $\phi$  depend in turn on  $\chi, \xi$  and  $\gamma$ . To make this dependence explicit, let us consider Figure 4, that shows, in the LOS reference frame, the path of a photon emitted from a point of the surface characterized by the polar angles  $\Theta_S$  and  $\Phi_S$ , up to the point where it crosses the adiabatic boundary, characterized by the angles  $\Theta$  and  $\Phi$ . Observing the star at infinity, one collects only photons that travel along vectors  $\mathbf{k} = (0, 0, k)$  parallel to the LOS  $\ell$ . The modulus of each vector  $\mathbf{k}$  is fixed by the condition:

$$\mathbf{r}_0 + \mathbf{k} = \mathbf{r}_a, \quad (20)$$

where  $\mathbf{r}_0 = R_{\text{NS}}(\sin \Theta_S \cos \Phi_S, \sin \Theta_S \sin \Phi_S, \cos \Theta_S)$  is the position vector of the surface point from which the photon has been emitted and  $\mathbf{r}_a = r_a(\sin \Theta \cos \Phi, \sin \Theta \sin \Phi, \cos \Theta)$  is the position vector of the point where the photon crosses the adiabatic boundary. Taking the norm of both the sides of equation (20) and solving for  $k$ , the only acceptable solution is

$$k = \sqrt{r_a^2 - R_{\text{NS}}^2 \sin^2 \Theta_S - R_{\text{NS}} \cos \Theta_S} \quad (21)$$

and, substituting this result again in equation (20), one obtains:

$$\mathbf{r}_a = \begin{pmatrix} R_{\text{NS}} \sin \Theta_S \cos \Phi_S \\ R_{\text{NS}} \sin \Theta_S \sin \Phi_S \\ \sqrt{r_a^2 - R_{\text{NS}}^2 \sin^2 \Theta_S} \end{pmatrix}, \quad (22)$$

where the distance  $r_a$  of the adiabatic boundary is given by equation (2). From simple geometrical considerations (see again Figure 3b), it follows that

$$\cos \theta = \mathbf{b}_{\text{dip}} \cdot \frac{\mathbf{r}_a}{r_a}, \quad (23)$$

while the cosine of the angle  $\phi$  can be obtained as

$$\cos \phi = \mathbf{p} \cdot \mathbf{r}_a^\perp, \quad (24)$$

where  $\mathbf{r}_a^\perp$  is the unit vector of the projection of  $\mathbf{r}_a$  orthogonal to

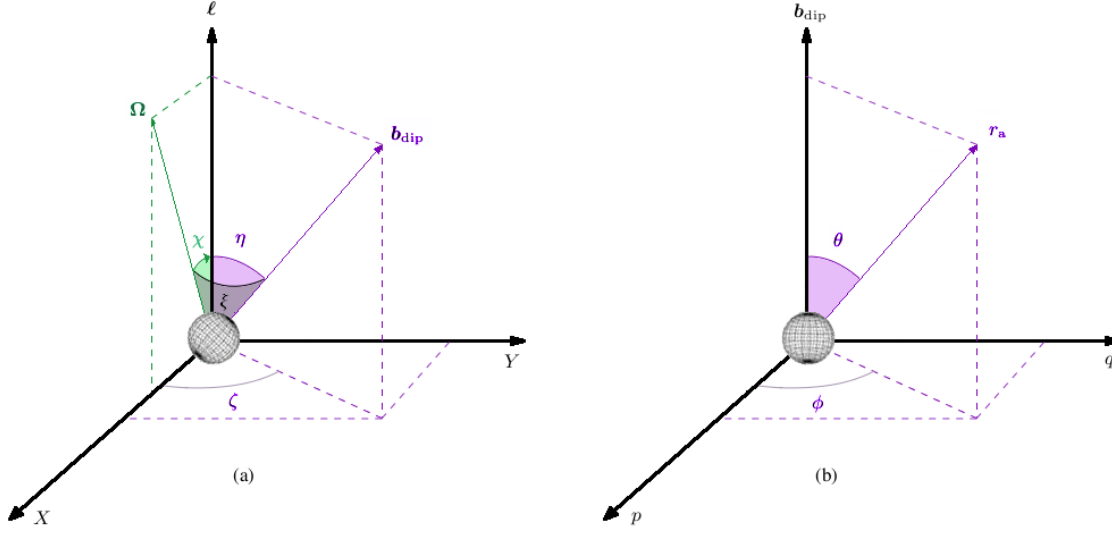


**Figure 3.** The two reference frames used in the calculation of the  $\alpha$  angle. *Left:* the  $(X, Y, Z)$  frame with the  $Z$  axis in the direction of the LOS  $\ell$ , the  $X$  axis in the plane  $\ell$ - $\Omega$ , where  $\Omega$  is the star spin axis, and the  $Y$  axis perpendicular to both  $X$  and  $Z$ . *Right:* the  $(p, q, t)$  reference frame with the  $t$  axis along the star magnetic axis  $\mathbf{b}_{\text{dip}}$ , the  $p$  and  $q$  two mutually orthogonal axes in the plane perpendicular to  $\mathbf{b}_{\text{dip}}$  (see Appendix B for more details). The angles  $\xi$ ,  $\chi$ ,  $\eta$ ,  $\theta$  and  $\phi$  are also shown.

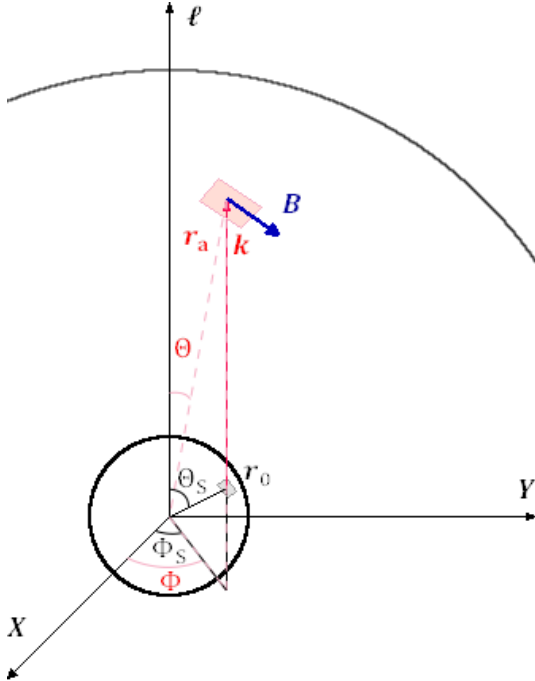


**Figure 4.** The path of a photon emitted by a point on the star surface with polar angles  $\Theta_S$  and  $\Phi_S$ , that crosses the adiabatic boundary in a point of polar coordinates  $\Theta$  and  $\Phi$ .

$\mathbf{b}_{\text{dip}}$ . The complete expressions of  $\cos \theta$  and  $\cos \phi$  are given in Appendix C.

Finally, substituting into equation (16) gives the distribution of  $\alpha$

$$\cos \alpha = \frac{B_X \sin \psi - B_Y \cos \psi}{\sqrt{B_X^2 + B_Y^2}}, \quad (25)$$

which is a function of the angles  $\chi$ ,  $\xi$ , the phase  $\gamma$ , the photon energy  $E$  and  $B_P$  (through the adiabatic radius  $r_a$ , see equation 2), the polar angles  $\Theta_S$  and  $\Phi_S$  that fix the point on the surface from which the photons were emitted and the angle  $\psi$  by which the polarimeter frame is rotated wrt the LOS one. In the following we take  $\psi = 0$ , i.e. the  $u$  ( $v$ ) axis coincides with the  $X$  ( $Y$ ) axis, although the generalization to other values is straightforward.

### 3.2 Numerical implementation

In order to calculate the polarization fraction  $\Pi_L$  and the polarization angle  $\chi_P$ , we use the ray-tracing code developed by Zane & Turolla (2006), with the addition of a specific module for the evaluation of the  $\alpha$  angle distribution and of the Stokes parameters. QED effects are included as described in section 2. The code takes also into account the effects due to the strong gravity on photon propagation (relativistic ray-bending) and on the stellar magnetic field. For a dipole field (see equations 17), the latter are given by

$$\begin{aligned} B_r^{\text{GR}} &= f_{\text{dip}} B_r \\ B_\theta^{\text{GR}} &= g_{\text{dip}} B_\theta \\ B_\phi^{\text{GR}} &= B_\phi = 0, \end{aligned} \quad (26)$$

where

$$\begin{aligned} f_{\text{dip}} &= -\frac{3}{x^3} \left[ \ln(1-x) + \frac{1}{2}x(x+2) \right] \\ g_{\text{dip}} &= \sqrt{1-x} \left( -2f_{\text{dip}} + \frac{3}{1-x} \right), \end{aligned} \quad (27)$$

with  $x = R_s/r$ ;  $R_s = 2GM_{\text{NS}}/c^2$  is the Schwarzschild radius and  $M_{\text{NS}}$  is the stellar mass (see Page & Sarmiento 1996).

The expressions for the total Stokes parameters  $Q$  and  $U$  given in equations (6) can be easily generalized to a continuous photon distribution by replacing the sums with integrals over the visible

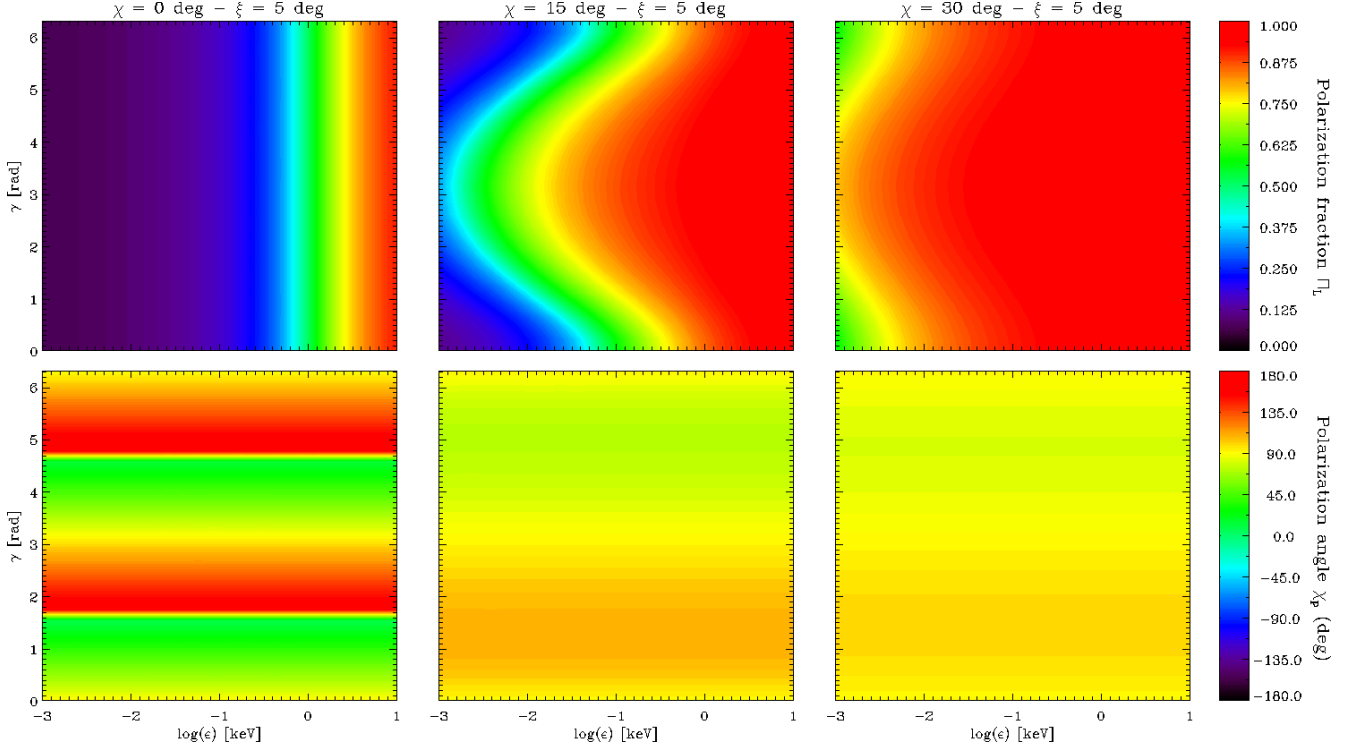


**Figure 5.** Contour plots in the energy-phase plane of the polarization fraction (top row) and the polarization angle (bottom row) for a neutron star with  $B_P = 10^{13}$  G,  $R_{\text{NS}} = 10$  km and mass  $M_{\text{NS}} = 1.4 M_{\odot}$ . The inclination of the magnetic axis with respect to the spin axis is fixed to  $\xi = 5^\circ$ , while the angle between the spin axis and the LOS is  $\chi = 0^\circ$  (left column),  $15^\circ$  (middle column) and  $30^\circ$  (right column). Seed photons are 100% polarized in the X-mode.

part of the star surface

$$\begin{aligned} F_Q &= \int_0^{2\pi} d\Phi_S \int_0^1 du^2 (n_X - n_O) \cos(2\alpha) \\ F_U &= \int_0^{2\pi} d\Phi_S \int_0^1 du^2 (n_O - n_X) \sin(2\alpha), \end{aligned} \quad (28)$$

where  $n_X$  ( $n_O$ ) is the photon intensity in the extraordinary (ordinary) mode and  $F_Q$  and  $F_U$  are the “fluxes” of the Stokes parameters (see Pavlov & Zavlin 2000). In general,  $n_X$  and  $n_O$  depend on the photon energy  $E$  and direction, and on the position on the star surface of the emission point. The integration variable  $u = \sin \bar{\Theta}$  is related to  $\Theta_S$  by the integral (see Zane & Turolla 2006, and references therein):

$$\bar{\Theta} = \int_0^{1/2} \frac{dv \sin \Theta_S}{[(1-x)/4 - (1-2vx)v^2 \sin^2 \Theta_S]^{1/2}}, \quad (29)$$

that accounts for ray-bending and reduces to  $\bar{\Theta} = \Theta_S$  in the limit  $x \rightarrow 0$  (when the effects of general relativity can be neglected). The total photon flux is obtained in a similar way

$$F_I = \int_0^{2\pi} d\Phi_S \int_0^1 du^2 (n_X + n_O). \quad (30)$$

For the sake of simplicity, we assume in the following that radiation is emitted by the cooling star surface with an isotropic blackbody distribution. The photon intensity is then

$$n_{X,O} = \frac{2}{h^2 c^2} \frac{E^2}{e^{E/kT} - 1}, \quad (31)$$

where  $T$  is the local surface temperature. In order to model the

surface thermal distribution and to avoid a vanishing temperature at the equator, here we adopt a variant of the standard temperature distribution for a core-centred dipole field (e.g. Page 1995),  $T(\vartheta) = \max(T_p |\cos \vartheta|^{1/2}, T_e)$ , where  $\vartheta$  is the angle between the local normal and  $\mathbf{B}$ ,  $T_p$  and  $T_e$  are the temperature at the pole and at the equator, respectively; in the following we take  $T_p = 150$  eV and  $T_e = 100$  eV. The polarization degree of the radiation emitted at the surface is fixed specifying the ratio  $p_0 = n_X/(n_X + n_O)$ ,  $|n_X - n_O|/(n_X + n_O) = |2p_0 - 1|$ .

### 3.3 Results

The polarization observables  $\Pi_L$  and  $\chi_P$  can be computed recalling the definitions given in equation (7) and using the expressions we just derived for the Stokes parameters, equations (28) and (30), together with the distribution of  $\cos \alpha$  given in equation (25). All results presented in this section refer to a neutron star with mass  $M_{\text{NS}} = 1.4 M_{\odot}$  and radius  $R_{\text{NS}} = 10$  km. Thermal photons are assumed to be 100% polarized in one of the two modes, i.e.  $p_0 = 0, 1$ ; essentially we consider all the photons as extraordinary, unless explicitly stated otherwise (see e.g. the discussion in Fernández & Davis 2011; Taverna et al. 2014). This is the choice which produces the most unfavourable conditions to detect the depolarizing effects of vacuum polarization and geometry on the polarization observables.

Figure 5 shows the polarization fraction and the polarization angle as functions of the photon energy and the rotational phase for different values of the inclination  $\chi$  of the LOS wrt the star spin axis. The magnetic axis is at an angle  $\xi = 5^\circ$  with respect to the spin axis (i.e. the NS is a nearly aligned rotator) and  $B_P = 10^{13}$



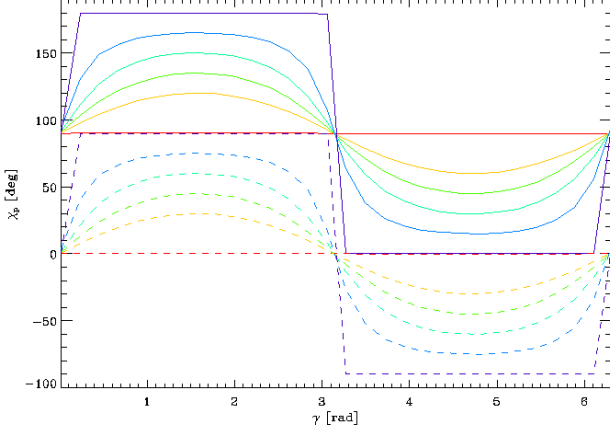


**Figure 6.** Polarization angle as a function of the rotational phase at a fixed energy ( $E = 0.02$  keV), for  $\chi = 90^\circ$  and different values of  $\xi$ :  $0^\circ$  (red),  $30^\circ$  (orange),  $45^\circ$  (green),  $60^\circ$  (light blue),  $75^\circ$  (blue) and  $90^\circ$  (violet). The solid (dashed) lines correspond to seed photons 100% polarized in the X-mode (O-mode). The values of  $R_{\text{NS}}$ ,  $M_{\text{NS}}$  and  $B_{\text{P}}$  are the same as in Figure 5.

G. The effects produced by the frame rotation (induced by the non-uniform  $B$ -field) are quite dramatic, as it is evident from the polarization fraction (top row). In particular, for  $\chi = 0$  (top left panel)  $\Pi_L$  is almost everywhere far from unity, the value expected from the intrinsic degree of polarization,  $|n_X - n_O|/(n_X + n_O) = 1$ , and it becomes  $\sim 0.9$  only at  $E \sim 10$  keV. By increasing the LOS inclination ( $\chi = 15^\circ$ , top middle panel), the polarization fraction reaches unity for photon energies  $\gtrsim 1$  keV, while at lower energies it is substantially smaller (between  $\sim 0.1$  and  $\sim 0.8$ ). Only when  $\chi$  becomes sufficiently large ( $\chi = 30^\circ$ , top right panel)  $\Pi_L$  is unity, except at low energies ( $\sim 1$ – $10$  eV), where the polarization fraction drops to about 0.6 in some phase intervals.

The bottom row of Figure 5 shows  $\chi_P$  for the same three simulations. Contrary of what happens for the polarization fraction, the polarization angle does not depend on the energy and exhibits an oscillatory behavior as a function of the rotational phase around a value of  $90^\circ$ . The amplitude of the oscillations depends on the geometrical angles and, for some combinations of  $\chi$  and  $\xi$ ,  $\chi_P$  sweeps the entire range  $[0^\circ, 180^\circ]$  through a discontinuity, or “jump”. This is clearly seen in the bottom left panel of Figure 5 where  $\chi = 0$ , while  $\chi_P$  is in between  $\sim 70^\circ$ – $110^\circ$  (bottom middle panel) and  $\sim 80^\circ$ – $100^\circ$  (bottom right panel) for  $\chi = 15^\circ$  and  $\chi = 30^\circ$ , respectively. This is further illustrated in Figure 6, which shows the polarization angle as a function of the rotational phase at a single energy ( $E = 0.02$  keV),  $\chi = 90^\circ$  and different values of  $\xi$  for radiation 100% polarized in the X-mode (solid lines) and in the O-mode (dashed lines). The amplitude of the oscillation vanishes in the case of an aligned rotator seen equator-on ( $\chi = 90^\circ$ ,  $\xi = 0^\circ$ ) and increases for increasing  $\xi$  until the “jump” appears for  $\xi = 90^\circ$ <sup>6</sup>. The average value of  $\chi_P$ , instead, does not change with  $\chi$  and  $\xi$  and is fixed by the polarization mode of the seed photons: it is  $90^\circ$  for X-mode photons and  $0^\circ$  for O-mode ones<sup>7</sup>. It should be noted,

however, that the mean value of the polarization angle is not univocally associated to the two photon modes, since it depends on the choice of the fixed reference frame  $(u, v, w)$ , i.e. on the angle  $\psi$  introduced in §3.1. If, for instance,  $\psi = 90^\circ$  (so that the  $u$  axis coincides with the  $Y$  axis of the LOS reference frame), the situation depicted in Figure 6 is reversed, with the polarization angle for X-mode photons oscillating around  $0^\circ$  and that for the O-mode ones around  $90^\circ$ . Of course, different choices of the  $\psi$  angle do not affect the polarization degree  $\Pi_L$ , the amplitude of the oscillations of  $\chi_P$  and the shift of  $90^\circ$  between the mean values of  $\chi_P$  for X-mode and O-mode photons.

The behaviour of the phase-averaged polarization fraction as a function of the angles  $\chi$ ,  $\xi$  is shown in Figure 7 for two values of the energy,  $E = 2$  eV (optical) and  $E = 0.3$  keV (X-rays). The right panel illustrates the variation of the semi-amplitude of  $\chi_P$ . As already noted by Fernández & Davis (2011), the amplitude is  $180^\circ$  for  $\xi \lesssim \chi$  when the phase-averaged polarization degree attains its minimum value (see §4).

The effects of varying the magnetic field strength are illustrated in Figure 8, where  $\chi = 15^\circ$ ,  $\xi = 5^\circ$  and  $B_P = 10^{12}$  G (left panel),  $B_P = 10^{13}$  G (middle panel; this is the same case shown in Figure 5) and  $B_P = 10^{14}$  G (right panel). Again, changes are mostly in the polarization fraction  $\Pi_L$  (top row). Overall, the polarization fraction is smaller when the magnetic field is lower (top left panel), and increases for increasing  $B_P$ , reaching values  $\sim 1$  (i.e. the intrinsic polarization degree) in almost the entire energy range for  $B_P = 10^{14}$  G (top right panel), see §4. On the contrary, the polarization angle (bottom row) does not change much, exhibiting an oscillation between  $\sim 70^\circ$  and  $\sim 110^\circ$  at all the values of  $B_P$ .

Finally, Figure 9 illustrates the effects on the polarization observables induced by the presence of a toroidal field component. The right column shows the phase-energy contour plot of the polarization fraction (top panel) and a phase plot of the polarization angle at a fixed energy<sup>8</sup> (bottom panel) for a globally twisted dipole field. The left column shows for comparison the same quantities for a pure dipole with the same  $B_P = 10^{13}$  G. The twisted magnetic field was evaluated using the analytical approximation by Pavan et al. (2009, see expressions in their Appendix A), with a twist angle  $\Delta\phi_{N-S} \simeq 50^\circ$ . Since relativistic corrections are unavailable for a twisted field, they were not applied also to the dipole we show for comparison, whereas ray bending is still considered in both the cases. The effects of the twist on the polarization fraction are quite modest and the variation of  $\Pi_L$  with photon energy and rotational phase is nearly the same as in the pure dipole case. The only difference is in a slight overall decrease in the polarization degree.

The twist of the external field affects much more the polarization angle, as it can be seen from the bottom row of Figure 9. The net effect is an overall asymmetry of the oscillations:  $\chi_P$  sweeps a larger angle in a half-period with respect to the purely dipolar case; this effect increases with the twist angle  $\Delta\phi_{N-S}$ , as already noticed by Fernández & Davis (2011).

have opposite signs and the polarization observables are obtained by summing the Stokes parameters over all photons, the mean value of  $\chi_P$  reflects the polarization mode which dominates.

<sup>8</sup> The twisted field actually introduces a dependence of  $\chi_P$  on the photon energy. For the values of the twist angle we consider, however, this dependence is quite small.

<sup>6</sup> The curves for  $\xi = 90^\circ$  in Figure 6 are box-like; the sloping lines are an artifact introduced by the finite resolution of the phase grid.

<sup>7</sup> Actually the mean value is the same even if photons are not all polarized in the same mode; since the Stokes parameters for O- and X-mode photons



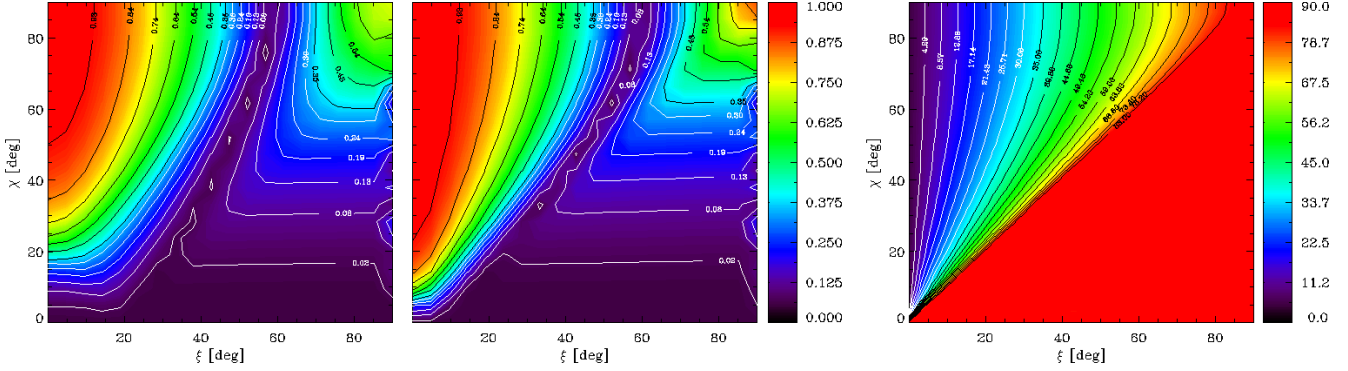


**Figure 7.** Contour plots for the phase-averaged polarization fraction at optical (2 eV, left panel) and X-ray (0.3 keV, middle panel) energies, and of the semi-amplitude of the oscillations of the polarization angle (right panel), as functions of  $\chi$  and  $\xi$ . The values of  $R_{\text{NS}}$ ,  $M_{\text{NS}}$  and  $B_{\text{P}}$  are the same as in Figure 5.

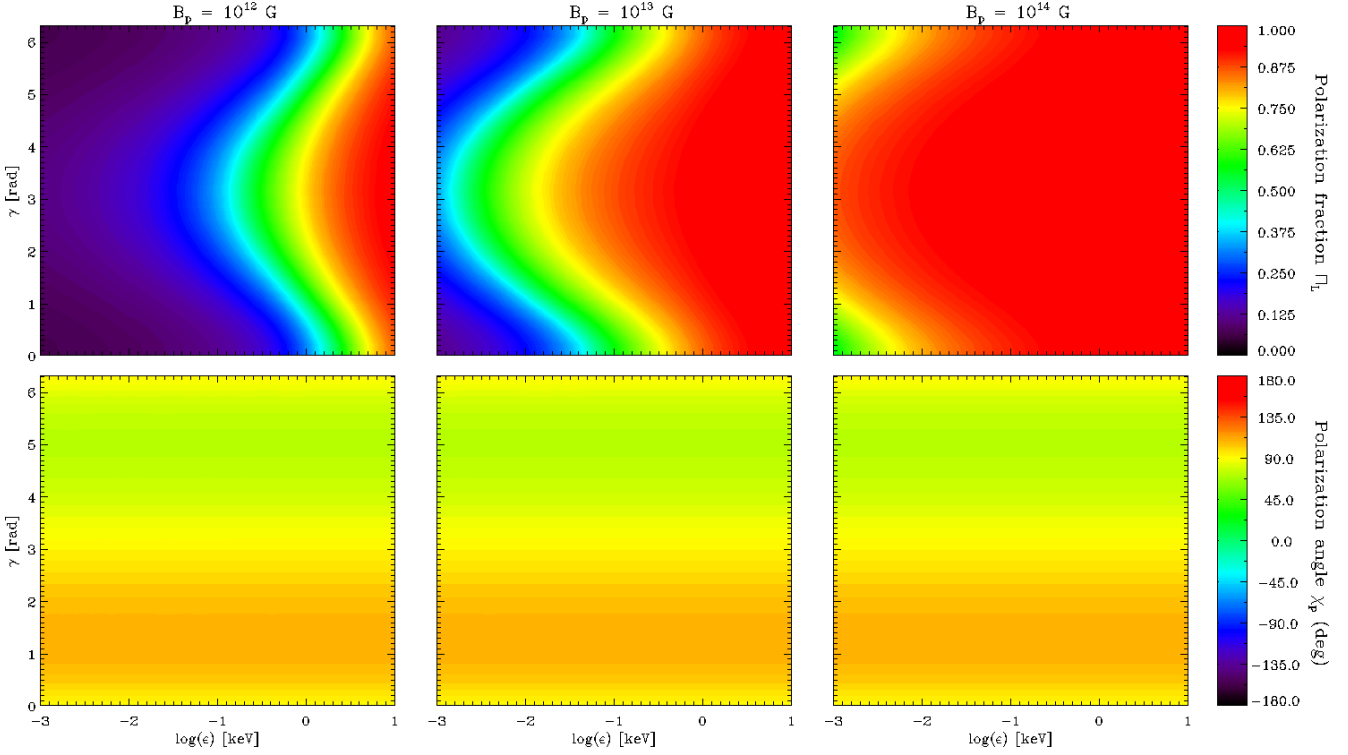


**Figure 8.** Same as in Figure 5 for  $\chi = 15^\circ$ ,  $\xi = 5^\circ$  and three different values of the magnetic field:  $B_{\text{P}} = 10^{12}$  (left column),  $10^{13}$  (middle column) and  $10^{14}$  G (right column).

#### 4 DISCUSSION AND CONCLUSIONS

In this paper we reconsidered the problem of the relation between the intrinsic and observed polarization properties in the case of surface emission from a neutron star. Our work extends previous investigations (Heyl, Shaviv & Lloyd 2003; Lai & Ho 2003; van Adelsberg & Perna 2009) by providing the polarization observables for a large set of physical and geometrical parameters (i.e. the angles  $\chi$  and  $\xi$ , the photon energy and the magnetic field strength and topology). Our treatment includes both “geometrical” effects, due to the rotation of the Stokes parameters which is needed when the magnetic field is not constant across the emitting region, and “vacuum polarization” (Heyl & Shaviv 2002); in order to make a full exploration of the parameter space possible, an approximated

treatment of QED was used. This resulted in much shorter computational times, without loosing significant physical accuracy, as the comparison with available results shows (Heyl, Shaviv & Lloyd 2003). We checked that a typical run required about 100 minutes integrating equations (1) and only few tens of seconds using our approximation. Moreover, our approach allows to better disentangle the effects of QED and those due to the rotation of the Stokes parameters on the polarization signals. We stress that our main goal was not to compute polarization observables for a precise, physical model of surface emission, but to systematically illustrate the role of these two effects in making polarization patterns different from those of the original radiation. To this end we assumed a quite simple picture in which the star magnetic field is a dipole and each

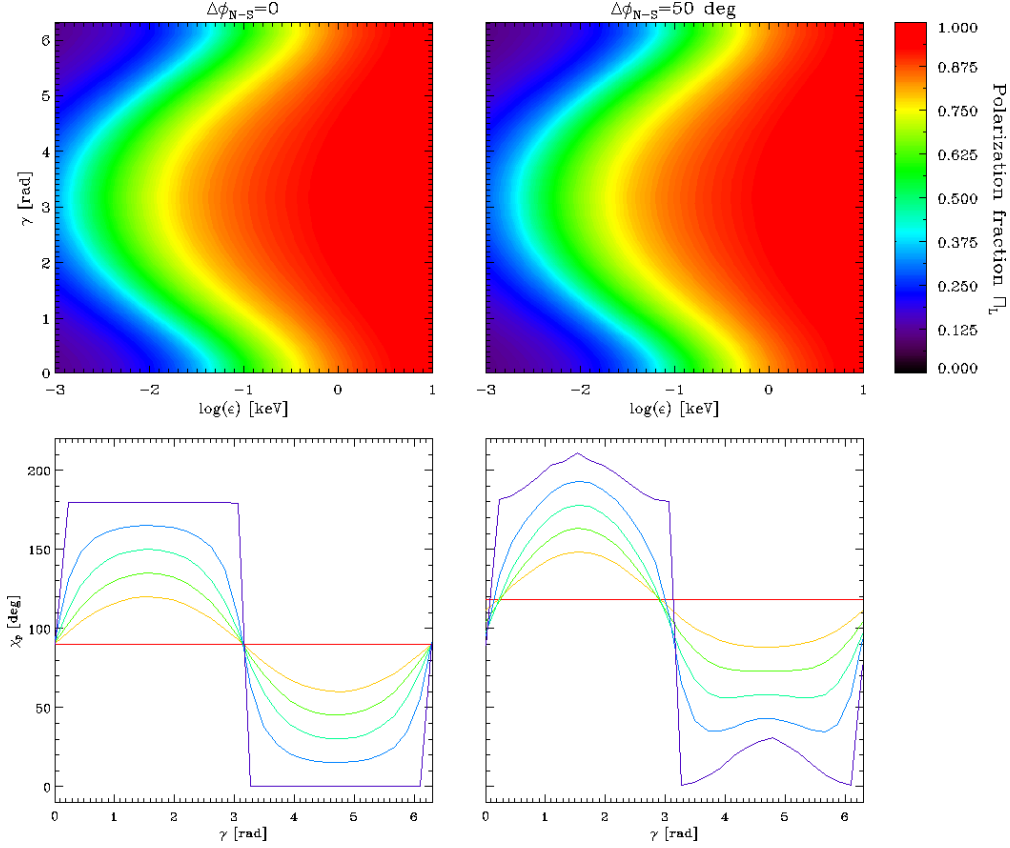


**Figure 9.** Polarization observables for the cases of a pure dipolar magnetic field (left column) and a globally twisted dipole with twist angle  $\Delta\phi_{N-S} \simeq 50^\circ$  (right column). Top row: polarization fraction in the energy-phase plane for  $\chi = 15^\circ$  and  $\xi = 5^\circ$ . Bottom row: polarization angle as a function of the rotational phase for a fixed photon energy ( $E = 0.02$  keV),  $\chi = 90^\circ$  and  $\xi = 0^\circ$  (red),  $30^\circ$  (orange),  $45^\circ$  (green),  $60^\circ$  (light blue),  $75^\circ$  (blue) and  $90^\circ$  (violet). All the plots are obtained for seed photons 100% polarized in the X-mode and values of  $R_{NS}$ ,  $M_{NS}$  and  $B_P$  as in Figure 5.

surface patch emits a (isotropic) blackbody spectrum at the local temperature. Our results can be easily generalized to other magnetic configurations (the case of a globally twisted field is actually discussed here) and to different surface emission models. A (comparative) analysis of the polarization observables for emission from an atmosphere (van Adelsberg & Lai 2006, and references therein) or from a condensed surface (Potekhin et al. 2012, and references therein) will be the subject of a future paper (Gonzalez Caniulef et al., in preparation).

A crucial point in assessing the measured polarization properties is that the polarization state of a photon propagating in a magnetized vacuum (either ordinary or extraordinary) is strictly related to the choice of the reference frame. In fact, the photon polarization mode is defined only with respect to the plane fixed by the wavevector and the local magnetic field. This means that the Stokes parameters of each photon are in general referred to different frames, with the two axes orthogonal to the direction of propagation tailored on the direction of the local  $B$ -field (§2.2). However, photons are collected in the focal plane of an instrument, where a reference direction has been a priori introduced. This means that in order to obtain the polarization observables relative to the photons received by the instrument in a given exposure time, the Stokes parameters of each photon must be transformed to the polarimeter reference frame, through a rotation in the plane orthogonal to the line-of-sight by an angle  $\alpha$ , which depends on the magnetic field

and viewing geometry, on the photon energy and on the position of the point from which photons were emitted (§3.1).

The effects induced by rotation of the reference frames compound those of vacuum polarization. According to QED, in fact, photons maintain their initial polarization state within the adiabatic region, while the polarization freezes at a larger distance (see §2.1). Despite the transition between the adiabatic and the outer zones is smooth, we assumed that there is a sharp boundary at the adiabatic radius  $r_a$  (see equation 2). This enabled us to treat the photons as if they were emitted at  $r_a$ , as far as their polarization state is concerned. This implies that the distribution of the  $\alpha$  angles, by which each frame has to be rotated, is actually determined by the magnetic field at the adiabatic radius, and hence depends also on the distance  $r_a$  from the star surface.

Simulations of polarization measurements (§3.3) clearly show that, because of the combined effects of frame rotation and QED, the measured polarization fraction can be very different from the intrinsic value, i.e. that of the radiation emitted at the surface. The differences appear to depend firstly on the viewing geometry, i.e. on the angles  $\chi$  and  $\xi$  which give the inclination of the line-of-sight and of the dipole axis with respect to the star spin axis. As shown in Figure 5, the polarization dramatically decreases at all rotational phases for  $\chi \simeq \xi \simeq 0$ . For  $\chi$  not too close to  $\xi$ ,  $\Pi_L$  has a minimum at the phase  $\gamma$  where the magnetic axis  $\mathbf{b}_{\text{dip}}$  lies in the plane of the rotation axis and the LOS (either  $\gamma = 0$  or  $2\pi$  with our choice of the reference frame). This behaviour confirms

the results of Heyl, Shaviv & Lloyd (2003) and it is entirely due to the non-constant magnetic field across the emitting region: when a region of the star near to the magnetic poles is into view, the projection of  $\mathbf{B}$  in the plane orthogonal to the LOS is essentially radial, so that  $\alpha$  can take values in the entire range  $[0, 2\pi]$ . Since the Stokes parameters for the whole radiation are obtained integrating the rotated Stokes parameters of single photons over the part of the star in view (see equations 28), the polarization degree has a minimum when the angle between  $\mathbf{b}_{\text{dip}}$  and the LOS is minimum (and equal to  $|\chi - \xi|$ , see the first of equations 12). On the other hand, the fact that  $\Pi_L$  does not change with rotational phase in the case shown in the top-left panel of Figure 5, is precisely due to the fact that this is a nearly aligned rotator viewed along the rotational axis.

In agreement with the results by Heyl, Shaviv & Lloyd (2003), we found that the behavior of  $\Pi_L$  is also sensitive to the location of the adiabatic radius. From the top rows of Figures 5 and 8, it can be seen that the linear polarization fraction increases with the photon energy and the polar strength of the  $B$ -field: this reflects the dependence of  $r_a$  on  $E^{1/5} B_P^{2/5}$ . In fact, as equation (25) shows,  $\cos \alpha$  depends on the magnetic co-latitude and azimuth,  $\theta$  and  $\phi$ , through  $B_X, B_Y$ ; the two latter angles contain the factor  $R_{\text{NS}}/r_a$  (see equations C1 and C3). So, in the limit  $r_a \gg R_{\text{NS}}$  (at least for axisymmetric magnetic field topology),  $\alpha$  remains nearly constant as the emission point changes on the star surface, implying that the polarization fraction can be indeed approximated with  $|n_X - n_O|/(n_X + n_O)$ , as equation (8) shows. Heyl, Shaviv & Lloyd (2003) explained this behavior as due to the fact that, in this limit, QED birefringence aligns the photon polarization angles. Actually, the weaker depolarization when  $r_a \gg R_{\text{NS}}$  is due chiefly to the rotation of the Stokes parameters, vacuum polarization entering only implicitly through the dependence of the angle  $\alpha$  on  $r_a$ . Because of the dependence of  $r_a$  on  $E$  and  $B_P$ , this approximation becomes better the larger the photon energy and the stronger the polar  $B$ -field. Instead, the closer to the star surface the adiabatic limit, the smaller the overall measured polarization degree, the latter becoming vanishingly small if no adiabatic region is accounted for. So, the main conclusion is the more point-like the star is seen by an observer at the adiabatic boundary, the closer the measured  $\Pi_L$  is to the intrinsic linear polarization degree. A similar effect was noted by Heyl, Shaviv & Lloyd (2003) in connection with the variation of the stellar radius.

On the other hand, the polarization angle exhibits quite a different behaviour. As Figures 5 and 8 show,  $\chi_p$  does not change significantly with  $r_a$ , since it does not depend on  $E$  and  $B_P$ . This is because the factors  $R_{\text{NS}}/r_a$  within  $\cos \alpha$  tend to cancel out taking the ratio  $U/Q$  which defines  $\chi_p$  (equation 7). The fact that  $\chi_p$  keeps oscillating even when the measured polarization fraction is much smaller than the intrinsic one (see bottom-left panels of Figures 5 and 8) is a consequence of the frame rotation and not of QED effects. The polarization angle depends quite strongly, instead, on the geometrical angles  $\chi$  and  $\xi$  (see e.g. the right panel of Figure 7). The polarization swing generally increases for decreasing  $\chi$  at fixed  $\xi$ , as shown in Figure 5. In particular,  $\chi_p$  sweeps the entire range  $[0, 180^\circ]$  when the region close to the magnetic pole is always in view during the star rotation (bottom left panel), while the swing gets smaller for values of  $\chi$  and  $\xi$  such that the polar region enters into view only at certain rotational phases. On the other hand, the oscillation amplitude in general grows for increasing  $\xi$  at fixed  $\chi$ . This behavior appears to be related again to the  $\alpha$ -angle distribution, and provides an explanation for the correlation between the swing by  $180^\circ$  of the polarization angle and the low phase-averaged

polarization fraction at  $\chi < \xi$ , as already noticed by Fernández & Davis (2011, see also Wagner & Seifert 2000). In fact, the regions where the polarization angle spans the widest range correspond to those in which at least one among the Stokes parameters  $Q$  and  $U$  takes all the values between  $-1$  and  $1$ . Consequently, the averaged polarization fraction, obtained by summing the Stokes parameters over a rotational cycle, turns out to be very small, as shown in Figure 7.

Phase-resolved polarization angle measurements, together with the information given by the linear polarization fraction, can help in understanding which polarization mode is the dominant one in the detected radiation. We showed in Figure 6 that the mean value of  $\chi_p$  depends on the mode in which the majority of photons are polarized. However, it is also related to the orientation of the  $(u, v)$  axes in the polarimeter plane (the  $\psi$  angle, see §3.1), which are fixed by the instrument design. In particular, the mean values of  $\chi_p$  for X- and O-mode photons are always displaced by  $90^\circ$ , but they are  $90^\circ$  and  $0^\circ$  respectively (as in the case in Figure 6) only if  $\psi = 0$ . Hence, a measurement of the polarization angle alone fails in telling which is the prevailing polarization mode. The problem can be solved if also a phase-resolved measurement of the linear polarization fraction is available. In this case, since  $\Pi_L$  has a minimum when  $\mathbf{b}_{\text{dip}}$  intercepts the  $\Omega - \ell$  plane (see above), it could indeed be possible to individuate the direction of the  $X$  axis on the plane of the sky. This allows to derive the angle  $\psi$  and to remove the inherent ambiguity in the measurement of  $\chi_p$ .

Polarization observables can also provide information on the source geometry, i.e. the inclination of the LOS and of the magnetic axis wrt the rotation axis. In fact, as discussed earlier on, both the polarization fraction and the polarization angle strongly depend on the angles  $\chi$  and  $\xi$ . As already shown in Taverna et al. (2014), if phase-resolved polarization signals are available, a simultaneous fit of  $\Pi_L$  and  $\chi_p$  (possibly supplemented by that of the flux) allows to unequivocally derive the values of  $\chi$  and  $\xi$ . On the contrary, this is in general not possible starting from phase-averaged measurements. The phase-averaged polarization fraction is largely degenerate with respect to the two angles, as clearly shown in Figure 7 and, since the phase average polarization angle is constant in large regions of the  $\chi - \xi$  plane, its measure is of no avail in pinpointing  $\chi$  and  $\xi$ .

The effects of a different magnetic field topology on the polarization observables were assessed in the illustrative case of globally-twisted dipolar magnetic field<sup>9</sup>. The presence of a toroidal component in the external magnetic field slightly changes the behaviour of linear polarization fraction (see Figure 9). In a twisted field, depolarization induced by the frame rotation is a bit stronger. This is due to the fact that  $B_{\text{twist}} > B_{\text{dip}}$  at any given position, because the toroidal component is roughly of the same order of the poloidal one, while the  $r$ -dependence is about the same for the two magnetic configurations. As a consequence the adiabatic boundary moves a bit closer to the surface if  $B_P$  and the photon energy are the same. A twisted field influences the polarization angle most, producing a strong asymmetry in the swing and a weak dependence on the energy (mainly at optical energies), as already discussed by Fernández & Davis (2011) and Taverna et al. (2014). The fact that the polarization angle is more sensitive to QED effects for a twisted

<sup>9</sup> We focused here only on surface emission, the interactions of photons with magnetospheric currents, chiefly through resonant cyclotron scattering, were ignored.

magnetosphere than for a purely dipolar field, provides a strong signature of vacuum polarization effects (see Taverna et al. 2014).

Our analysis further demonstrates the need to properly account for QED and frame rotation effects in evaluating the observed polarization properties of radiation emitted by a neutron star. This is of particular relevance in relation to recently proposed X-ray polarimetry missions, which will certainly select neutron star sources as primary targets.

## ACKNOWLEDGMENTS

It is a pleasure to thank Enrico Costa for many illuminating discussions, Kinwah Wu for some useful comments and an anonymous referee, whose helpful suggestions helped us in improving a previous version of the manuscript. The work of RT is partially supported by INAF through a PRIN grant. DGC acknowledges a fellowship from CONICYT-Chile (Becas Chile). He also acknowledges financial support from the RAS and the University of Padova for funding a visit to the Department of Physics and Astronomy, during which part of this investigation was carried out.

## REFERENCES

- Bellazzini R., Brez A., Costa E., Minuti M., Muleri F., Pinchera M., Rubini A., Soffitta P., Spandre G., 2013, NIMPA, 720, 173  
 Dean A. J., Clark D. J., Stephen J. B., McBride V. A., Bassani L., Bazzano A., Bird A. J., Hill A. B., Shaw S. E., Ubertini P., 2008, Science, 321:1183  
 Fabiani S., Muleri F., 2014, Astronomical X-Ray polarimetry (Ar-iccia: Aracne Ed.)  
 Fernández R., Davis S. W., 2011, ApJ, 730, 131  
 Gnedin Yu. N., Pavlov, G. G., 1974, Soviet Phys.-JETP Lett., 38, 903  
 Harding A. K., Lai D., 2006, Rep. Prog. Phys. 69, 2631  
 Heyl J.S., Shaviv N.J., 2000, MNRAS, 311, 555  
 Heyl J.S., Shaviv N.J., 2002, Phys. Rev. D, 66, 023002  
 Heyl J.S., Shaviv N.J., Lloyd D., 2003, MNRAS, 342, 134  
 Hughes J. P., Long K. S., Novick R., 1984, ApJ, 280, 255  
 Jahoda K. M., Kouveliotou C., Kallman T. R. et al., 2015, American Astronomical Society, AAS Meeting #225, #338.40  
 Kaspi V. M., 2010, PNAS, 107, 7147-7152  
 Kislat F., Clark B., Beilicke M., Krawczynski H., 2015, Astropart. Phys., 68, 45  
 Lai D., Ho W.C.G., 2003, Phys. Rev. Lett., 91, 071101  
 Lai D., Ho W. C. G., Van Adelsberg M., Wang C. & Heyl J.S., 2010, X-ray Polarymetry: A New Window in Astrophysics (Cambridge: Cambridge University Press)  
 Lyne A. G., Manchester R. N., 1988, MNRAS, 234, 477  
 Manchester R. N., Taylor J. H., 1977, Pulsars (San Francisco: Freeman)  
 Mereghetti S. 2008, A&A Rev., 15, 225  
 Nobili L., Turolla R., Zane S., 2008, MNRAS, 386, 1527  
 Page D. 1995, ApJ, 442, 273  
 Page D., Sarmiento A., 1996, ApJ, 473, 1067  
 Pavan L., Turolla R., Zane S., Nobili L., 2009, MNRAS, 395, 753  
 Pavlov G. G., Zavlin V. E., 2000, ApJ, 529, 1011  
 Potekhin A.Y., Suleimanov V.F., M. van Adelsberg, Werner K., 2012, A&A 546, A121  
 Rybicki, G. B., Lightman, A. P., 2004, Radiative Processes in Astrophysics (2nd ed.; Weinheim: Wiley)

- Taverna R., Muleri F., Turolla R., Soffitta P., Fabiani S., Nobili L., 2014, MNRAS, 438, 1686  
 Thompson C., Lyutikov M., Kulkarni S.R., 2002, ApJ, 574, 332  
 Trippe, S. 2014, JKAS, 47, 15  
 Turolla, R. 2009, ASSL, 357, 141  
 Turolla R., Zane S., Watts A. L., 2015, Rep. Prog. Phys., in press [arXiv:1507.02924]  
 van Adelsberg, M., Lai, D., 2006, MNRAS, 373, 1495  
 van Adelsberg, M., Perna, R., 2009, MNRAS, 399, 1523  
 Viganò D., Pons J. A., 2012, MNRAS, 425, 2487  
 Wagner S. J., Seifert W., 2000, Pulsar Astronomy – 2000 and Beyond, ASP Conference Series, Vol. 202, 315 (M. Kramer, N. Wex, and R. Wielebinski, eds.)  
 Wang C., Lai D., 2009, MNRAS, 398, 515  
 Weisskopf M.C., Silver E. H., Kastenbaum K. S., Long K. S., Novick R., Wolff R. S., 1978, ApJ, 220, L117  
 Weisskopf M. C. et al., 2013, Proc. SPIE 8859, UV, X-Ray, and Gamma-Ray Space Instrumentation for Astronomy XVIII, 885908  
 Wiktorowicz S., Ramirez-Ruiz E., Illing R. M. E., Nofi L., 2015, AAS Meeting, 225, 421.01  
 Zane S., Turolla R., 2006, MNRAS, 366, 727

## APPENDIX A: CARTESIAN COMPONENTS OF $\mathbf{B}$

The cartesian components of the magnetic field  $\mathbf{B}$  in the reference frame  $(p, q, t)$  can be obtained from its polar components  $\mathbf{B}^{\text{pol}} = (B_r, B_\theta, B_\phi)$  given in equation (17) using the following expression

$$\mathbf{B} = (B_p, B_q, B_t) = (\mathbf{B}^{\text{pol}} \cdot \mathbf{p}^{\text{pol}}, \mathbf{B}^{\text{pol}} \cdot \mathbf{q}^{\text{pol}}, \mathbf{B}^{\text{pol}} \cdot \mathbf{t}^{\text{pol}}), \quad (\text{A1})$$

where  $\mathbf{p}^{\text{pol}}$ ,  $\mathbf{q}^{\text{pol}}$  and  $\mathbf{t}^{\text{pol}}$  are the unit vectors relative to the  $(p, q, t)$  frame expressed in polar components

$$\begin{aligned} \mathbf{p}^{\text{pol}} &= \mathbf{p} \cdot (\hat{r}, \hat{\theta}, \hat{\phi}) = (\sin \theta \cos \phi, \cos \theta \cos \phi, -\sin \phi) \\ \mathbf{q}^{\text{pol}} &= \mathbf{q} \cdot (\hat{r}, \hat{\theta}, \hat{\phi}) = (\sin \theta \sin \phi, \cos \theta \sin \phi, \cos \phi) \\ \mathbf{t}^{\text{pol}} &= \mathbf{t} \cdot (\hat{r}, \hat{\theta}, \hat{\phi}) = (\cos \theta, -\sin \theta, 0), \end{aligned} \quad (\text{A2})$$

and the angles  $\theta$  and  $\phi$  are the magnetic colatitude and azimuth, respectively (see Figure 3b). Upon substituting expressions (A2) into equation (A1), one finally obtains

$$\begin{aligned} B_p &= \sin \theta \cos \phi B_r + \cos \theta \cos \phi B_\theta - \sin \phi B_\phi \\ B_q &= \sin \theta \sin \phi B_r + \cos \theta \sin \phi B_\theta + \cos \phi B_\phi \\ B_t &= \cos \theta B_r - \sin \theta B_\theta. \end{aligned} \quad (\text{A3})$$

## APPENDIX B: MAGNETIC REFERENCE FRAME

The projection of  $\mathbf{b}_{\text{dip}}$ , given by equation (13), orthogonal to the spin axis  $\boldsymbol{\Omega}$  (see §3.1), in the LOS reference frame  $(X, Y, Z)$  is

$$\mathbf{m} \equiv \frac{\mathbf{b}_{\text{dip}} - (\mathbf{b}_{\text{dip}} \cdot \boldsymbol{\Omega}) \boldsymbol{\Omega}}{|\mathbf{b}_{\text{dip}} - (\mathbf{b}_{\text{dip}} \cdot \boldsymbol{\Omega}) \boldsymbol{\Omega}|} = \begin{pmatrix} -\cos \chi \cos \gamma \\ \sin \gamma \\ \sin \chi \cos \gamma \end{pmatrix}; \quad (\text{B1})$$

$\mathbf{m}$  is an unit vector corotating with the star around the spin axis. The projection of  $\mathbf{m}$  perpendicular to  $\mathbf{b}_{\text{dip}}$  fixes the  $p$  axis of the  $\mathbf{b}_{\text{dip}}$  reference frame  $(p, q, t)$ . Its expression in the  $(X, Y, Z)$  frame

is given by

$$\begin{aligned} \mathbf{p} &\equiv \frac{\mathbf{m} - (\mathbf{m} \cdot \mathbf{b}_{\text{dip}})\mathbf{b}_{\text{dip}}}{|\mathbf{m} - (\mathbf{m} \cdot \mathbf{b}_{\text{dip}})\mathbf{b}_{\text{dip}}|} \\ &= \begin{pmatrix} -\sin \chi \sin \xi - \cos \chi \cos \xi \cos \gamma \\ \cos \xi \sin \gamma \\ \sin \chi \cos \xi \cos \gamma - \cos \chi \sin \xi \end{pmatrix}. \end{aligned} \quad (\text{B2})$$

Finally, the unit vector defining the  $q$  axis, in the  $(X, Y, Z)$  reference frame, is given by the vector product between  $\mathbf{b}_{\text{dip}}$  and  $\mathbf{p}$

$$\mathbf{q} = \mathbf{b}_{\text{dip}} \times \mathbf{p} = \begin{pmatrix} -\cos \chi \sin \gamma \\ -\cos \gamma \\ \sin \chi \sin \gamma \end{pmatrix}. \quad (\text{B3})$$

### APPENDIX C: COMPLETE EXPRESSIONS FOR $\cos \theta$ AND $\cos \phi$

Substituting the components of  $\mathbf{b}_{\text{dip}}$  (equation 13) and of  $\mathbf{r}_a$  (equation 22) into equation (23) one obtains

$$\begin{aligned} \cos \theta &= \frac{R_{\text{NS}}}{r_a} \sin \Theta_S \left( \cos \Phi_S \sin \chi \cos \xi + \sin \Phi_S \sin \xi \sin \gamma \right. \\ &\quad \left. - \cos \Phi_S \cos \chi \sin \xi \cos \gamma \right) \\ &\quad + \sqrt{1 - \left( \frac{R_{\text{NS}}}{r_a} \sin \Theta_S \right)^2} \left( \cos \chi \cos \xi + \sin \chi \sin \xi \cos \gamma \right). \end{aligned} \quad (\text{C1})$$

To calculate the complete expression of  $\cos \phi$  we use equation (24), where the components of the unit vector  $\mathbf{p}$  are given in equation (B2) and

$$\mathbf{r}_a^\perp = \frac{\mathbf{r}_a - (\mathbf{r}_a \cdot \mathbf{b}_{\text{dip}})\mathbf{b}_{\text{dip}}}{|\mathbf{r}_a - (\mathbf{r}_a \cdot \mathbf{b}_{\text{dip}})\mathbf{b}_{\text{dip}}|}. \quad (\text{C2})$$

Putting all together, one obtains

$$\begin{aligned} \cos \phi &= \frac{R_{\text{NS}} \sin \Theta_S}{r_a \sin \theta} \left( \sin \Phi_S \cos \xi \sin \gamma - \cos \Phi_S \sin \chi \sin \xi \right. \\ &\quad \left. - \cos \Phi_S \cos \chi \cos \xi \cos \gamma \right) \\ &\quad + \sqrt{\frac{r_a^2 - (R_{\text{NS}} \sin \Theta_S)^2}{r_a^2 \sin^2 \theta}} \left( \sin \chi \cos \xi \cos \gamma - \cos \chi \sin \xi \right). \end{aligned} \quad (\text{C3})$$